Research article

Glymphatic clearance of simulated silicon dispersion in mouse brain analyzed by laser induced breakdown spectroscopy

Muhammad Shehzad Khan [a,1], Rachit Kumar [b,1], Sinai H.C. Manno [a,c,1], Irfan Ahmed [d,1], Alan Wing Lun Law [a], Raul R. Cruces [e], Victor Ma [f], William C. Cho [f], Shuk Han Cheng [c,g,h], Condon Lau [a,*]

[a] Department of Physics, City University of Hong Kong, Kowloon, HKSAR, China
[b] Wallace H. Coulter Department of Biomedical Engineering, Georgia Institute of Technology and Emory University, Atlanta, GA, USA
[c] Department of Biomedical Sciences, College of Veterinary Medicine and Life Sciences, City University of Hong Kong, Kowloon, HKSAR, China
[d] Electrical Engineering Department, Sukkur IBA University, Sukkur 65200, Sindh, Pakistan
[e] McConnell Brain Imaging Center, Montreal Neurological Institute and Hospital, McGill University, Montreal, QC, Canada
[f] Department of Clinical Oncology, Queen Elizabeth Hospital, Kowloon, HKSAR, China
[g] State Key Laboratory of Marine Pollution (SKLMP), City University of Hong Kong, Kowloon, HKSAR, China
[h] Department of Materials Science and Engineering, City University of Hong Kong, Kowloon, HKSAR, China

ARTICLE INFO

ABSTRACT

Silicon-based devices, such as neural probes, are increasingly used as electrodes for receiving electrical signals from neural tissue. Neural probes used chronically have been known to induce inflammation and elicit an immune response. The current study detects and evaluates silicon dispersion from a concentrated source in the mouse brain using laser induced breakdown spectroscopy. Element lines for Si (I) were found at the injection site at approximately 288 nm at 3hr post-implantation, even with tissue perfusion, indicating possible infusion into neural tissue. At 24hr and 1-week post-implantation, no silicon lines were found, indicating clearance. An isolated immune response was found by CD68 macrophage response at 24hr post injection. Future studies should measure chronic silicon exposure to determine if the inflammatory response is proportional to silicon administration. The present type of protocol, coupling laser induced breakdown spectroscopy, neuroimaging, histology, immuno-histochemistry, and determination of clearance could be used to investigate the glymphatic system and different tissue states such as in disease (e.g. Alzheimer's).

1. Introduction

Neural probes constructed of silicon (and Si-based substrates, including elastomers such as poly-dimethylsiloxane- PDMS) have become increasingly common in electrophysiology (Buzsáki, 2015; Gunasekera et al., 2015; Jun et al., 2017; Rivnay et al., 2017). There has been considerable research and development into human chronic electrode implants using silicon as the candidate material (Kim et al., 2008; Hochberg et al., 2006, 2012; Collinger et al., 2013). Silicon has been used as the base for resorbable probes (Hwang et al., 2012; Kang et al., 2016; Yu et al., 2016), complementary metal-oxide-semiconductor (CMOS) multielectrode arrays (MEAs; Jun et al., 2017), micromachined shanks (Wise et al., 1970; Wise and Angell, 1975), silicon photodetectors for

stimulation (Mandel et al., 2013; Mathieson et al., 2012; Lorach et al., 2015) and for industry standard probes such as the Michigan (Wise et al., 1970; Wise and Angell, 1975; BeMent et al., 1986) and Utah arrays (Campbell et al., 1991; Gunasekera et al., 2015; Jorfi et al., 2015). There are three main issues to overcome and related goals to achieve in probe insertion to increase biocompatibility in neural interfaces: 1) Anti-corrosion, 2) anti-neuroinflammatory, and 3) prohibiting electrode performance diminishment (Gunasekera et al., 2015; Jun et al., 2017; Rivnay et al., 2017). The main advantages neural probes need to possess are low impedance, good surface adhesion, noncorrosive, anti-inflammatory response and sustained performance over insertion time (Gunasekera et al., 2015; Jun et al., 2017; Rivnay et al., 2017). Several studies have found device degradation and an acute immune

---

* Corresponding author.
E-mail address: condon.lau@cityu.edu.hk (C. Lau).
[1] Contributed equally.

response followed by chronic neuroinflammatory response associated with probes (Edell et al., 1992; Turner et al., 1999; Szarowski et al., 2003; Biran et al., 2005, 2007; Skousen et al., 2011). However, few protocols have assessed silicon dispersion into brain tissue from a concentrated source, such as probe insertion. Here, we describe an effective method of measuring silicon dispersion using laser induced breakdown spectroscopy (LIBS) verified by magnetic resonance imaging localization to assess possible infusion into neural tissue and neuroinflammatory response.

Spectroscopic techniques provide a fast identification of elements, facilitating the analysis of complex biological materials. LIBS has become an important tool due to the high resolution and real-time assessment of specific elements in different biological tissues (Rehse et al., 2012). In fact, some researchers (Teran-Hinojosa et al., 2017; Kumar et al., 2004) have used LIBS to characterize tissues for diagnosis of diseases such as fibrosis (Rehse et al., 2012) or to characterize certain pathogens (Mohaidat et al., 2012; Kim et al., 2004). The atomic emission lines obtained from the spectrum in LIBS permit the identification of elements while relative intensities are used to determine the relative concentrations of those corresponding elements. Yueh et al. (2009) used LIBS combined with chemometric techniques to differentiate tissue samples from each other, such as brain, lung, spleen, liver, kidney and skeletal muscle. Here, we used LIBS to observe and quantify the progression of silicon leaching into brain tissue from a concentrated source. Using LIBS to assess different tissue states has the potential for significant impact in the biomedical sciences.

Our aim for the present experiment was to investigate the dispersion of silicon from a concentrated source in the brain, such as a neural probe, subsequent infusion into neural tissue, and putative resultant inflammatory response. We used a longitudinal design by monitoring hours and days post silicon injection. We prepared tissue for histology (Luxol fast blue and Cresyl fast violet - Nissl) to confirm probe position, examined the inflammatory response present, used MRI to overlay histology and for localization and finally LIBS to quantify the elemental prescence of silicon per injection brain site. The main advantages of LIBS are easy sample preparation and effective spectroscopic elemental analysis of tissue samples. We have recently assessed a variety of tissues using LIBS coupling other techniques to determine elemental content during different biologically relevant states such as the effect of coffee on dental enamel (Ahmed et al., 2017; Ahmed et al., 2018a; Ahmed et al., 2018b; Manno et al., 2018).

2. Methods

See Figure 1 for detailed explanation of the experimental design.

2.1. Animal model of silicon dispersion

Mice C57BL/6 male, 8 weeks old were used. Groups consisted of 10 mice per regimen and time point, plus sham for a total of 60 mice. Mice were divided into 3 groups (3hr, 24hr, 1 week injection regimens), in addition to equal groups of saline injected controls for each time point for LIBS. For subsequent protocols with immunohistochemistry (IHC) and histology, mice were divided into 3 time point groups, 2 mice each in addition to controls. Silicon dispersion was initiated by injecting a silicon bolus into a specific region of interest (ROI). Injection coordinates of the simulated probe were ML: 1.50, AP: -4.70, DV: -2.50, the ventral aspect of the external cortex of the inferior colliculus (ECIC) in the left or right hemisphere, here our group are experts in IC localization (Dong et al.,
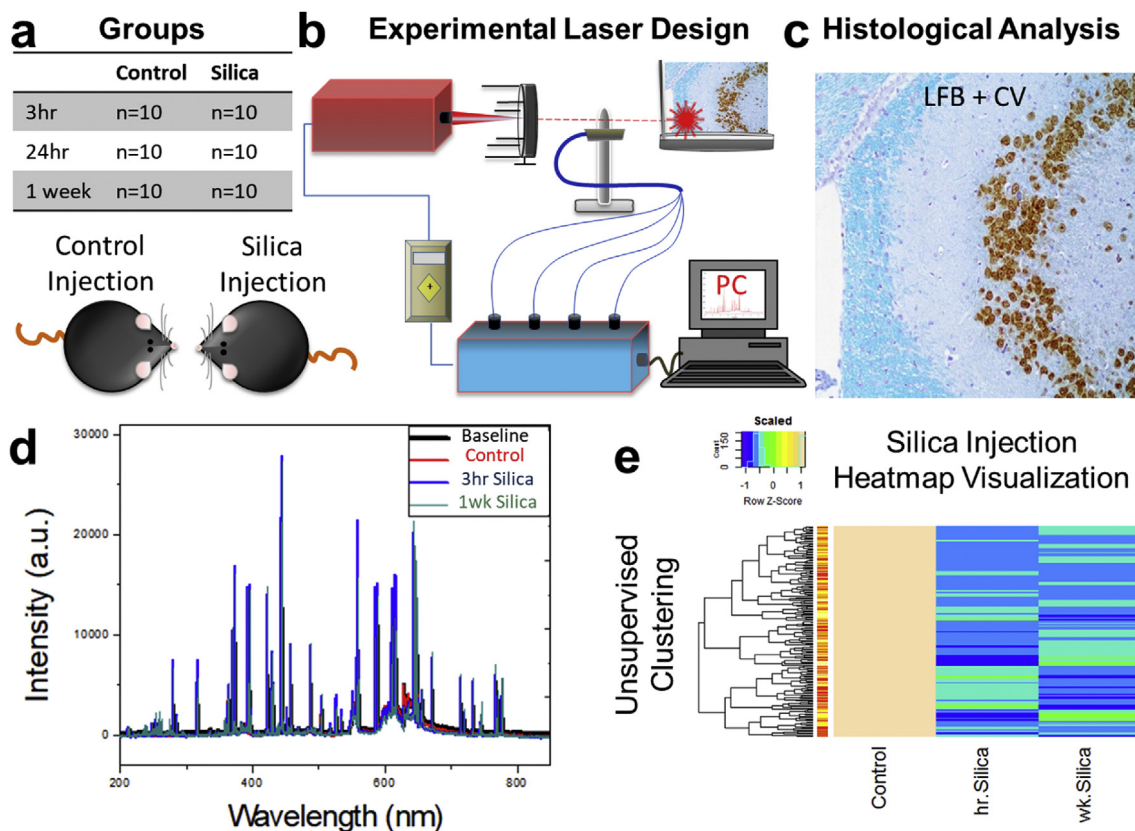

Figure 1. Experimental design. a) Experimental groups for analysis of simulated probe. b) Schematic diagram of the laser induced breakdown spectroscopy (LIBS) setup. The laser pulse is focused by the lens (L) onto the sample (Manno et al., 2018). The ablated portion of the sample emits light which is collected by the fiber and channeled to the spectrometer. The setup is controlled by a personal computer (PC), which triggers both the laser and the spectrometer. The resultant spectra is displayed which is analyzed and post-processed. c) Histological analysis consisting of by Luxol fast blue (LFB) and Cresyl violet (CV - Nissl). d) Resultant raw spectra obtained from different groups. e) Heatmap visualization for demonstration of differences in spectra.

2018). The present protocol is a rapid version of silicon degradation from a neural probe. The silicon bolus was 5 μl of supersaturated 5 mg Si (silicon) in 50 ml saline heated to 100 °C for 15 min and cooled for 15 min at 13 °C before injection at room temperature (Sigma Aldrich, Milwaukee, Wis., USA). After injection, mice were left to recover and subsequently examined by histological protocols or LIBS. To verify probe location and calculate diffusion from ROI site, magnetic resonance imaging (MRI) was used for in-vivo verification (Figure 2 – demonstrative) and histological analysis was used for neural damage analysis, respectively. Immunohistochemistry (IHC) and LIBS was shot on 50 μm prepared slices to determine cell damage and Si diffusion from ROI site, respectively. For IHC and histology, three-time points for the Si simulated probe and a saline control (saline) injection were utilized.

2.2. MRI probe location

Methods for MRI were based on our previous protocols (Lau et al., 2018; Dong et al., 2018; Manno et al., 2019; Wong et al., 2020). The injection needle was localized by structural MRI (sMRI) for in-vivo verification. Mice for sMRI were initially anesthetized with 5% isoflurane. Mice were placed on a holder in the prone position with a tooth bar to restrict head motion. Heart rate, respiration rate, and oxygen saturation were continuously monitored by MRI-compatible sensors (SA instruments) and kept in normal ranges (heart rate: 380–420; respiration rate: 59–61; oxygen saturation: > 95%). The sMRI was acquired using a Bruker ICON 1T scanner (Bruker Biospin GmbH) with a T1-weighted Rapid Acquisition with Refocused Echoes (RARE) image. Imaging used a transmit-only birdcage coil in combination with an actively decoupled receive-only surface coil. Scout images were first acquired to determine the coronal and sagittal planes of the brain. Five coronal slices 1.0 mm in thickness were positioned to cover the entire simulated probe location (AP = -4.70 mm Bregma, ML = 1.50mm, and DV = -2.50 mm Bregma) ventral aspect of ECIC left/right hemisphere, according to the mouse brain atlas (Franklin and Watson, 2008). Scanning parameters were echo time = 20 ms, rare factor = 4, repetition time = 922.938ms, repetitions = 8, flip angle = 90, resulting in a scan time of 5m32s257ms per animal. The image was isotropic in slice spatial resolution of 0.375 μm with 5 continuous slices at 1mm slice thickness, with spatial size phase = 180 pixels. Images were analyzed in ImageJ to localize the probe (Figure 2).

2.3. Immunohistochemistry, histology and paraffin preparation for LIBS

Injection location was confirmed using Orange Dye (Cancer Diagnostics, Inc, ref: 0728-6), a fluorescent stain (Jiang et al., 2017). Samples were prepared for either IHC and staining by Luxol fast blue, Cresyl fast violet (Nissl), or section blocking for LIBS shooting. For the first IHC experiment, the following was utilized: Anti-NeuN antibody (AB177487 abcam Rabbit monoclonal [EPR12763]), conjugated with secondary antibody Alexa Fluor 594nm (AB150064) Donkey Anti-Rabbit IgG H&L with Fluoroshield™ mounting medium fortified with counterstaining DAPI (AB104139); in a second IHC experiment, the following was utilized: Mouse monoclonal [ED1] to CD68 (AB31630), conjugated with Goat Anti-Mouse IgG H&L (Alexa Fluor® 488, AB150113), and Anti-GFAP antibody [EPR1034Y] (Alexa Fluor® 568, AB201736) counterstained using Rat monoclonal to Tubulin (Alexa Fluor® 647, AB195884), at 1/250 dilution with Fluoroshield™ mounting medium fortified with counterstaining DAPI (AB104139). Tissue was fixed by PBS perfusion with paraformaldehyde, with 10% serum for 1 h at 25 °C for heat mediated antigen retrieval Tris/EDTA buffer pH 9.0. The sample was incubated with primary antibody (1/500 in PBS +1% serum +0.1% Triton X-100) for 16 h at 25 °C and in the secondary antibody for 1 h. Tissue for generic histology was prepared for Luxol fast blue and Cresyl fast violet (Nissl). Tissue was dehydrated in 3 alcohol concentrations 70%–85% to 90%, placed in toluene, and paraffin wax infiltrated at 60 °C. Embedded tissue was oriented coronally and cut at 5–10 μm with a microtome and spread on a microscope slide. Sections were deparaffinized, and hydrated in distilled water. Slides were incubated in Luxol fast blue for 2 h at 60 °C and rinsed in distilled water. Sections were differentiated by dipping in lithium carbonate until a sharp contrast between the blue white-matter and colorless grey matter was apparent, succeeded by alcohol, and then rinsed in distilled water. Slides were then incubated in Cresyl echt violet for 2–5 min, rinsed in distilled water, and dehydrated in absolute alcohol (see histological protocol, Manno and Lau, 2018). For LIBS shooting, tissue was prepared by PBS perfusion and placed in paraformaldehyde. Mouse brains were transferred to a brain matrix (RWD Life Science 68707) in the coronal position, sectioned at 0.5 mm, mounted on slides, and oriented for left/right hemisphere LIBS shooting.

2.4. Laser induced breakdown spectroscopy of probe disintegration and localization

In brief (Ahmed et al., 2017; Ahmed et al., 2018a; Ahmed et al., 2018b; Manno et al., 2018), a 1064 nm pulse laser (CFR200, Quantel) emitting an 8 ns, 200 mJ pulse focused to a 10 μm spot was utilized for LIBS. All spectroscopic analysis was performed in standard atmospheric air. The optical emission from the tissue was collected by a six-channel fiber (2000 μm diameter) bundle positioned 35 mm from the focal point and at 45° from the laser beam. The fibers relayed light to six spectrometers spanning 200–900 nm with 0.1 nm resolution (MX2500 +
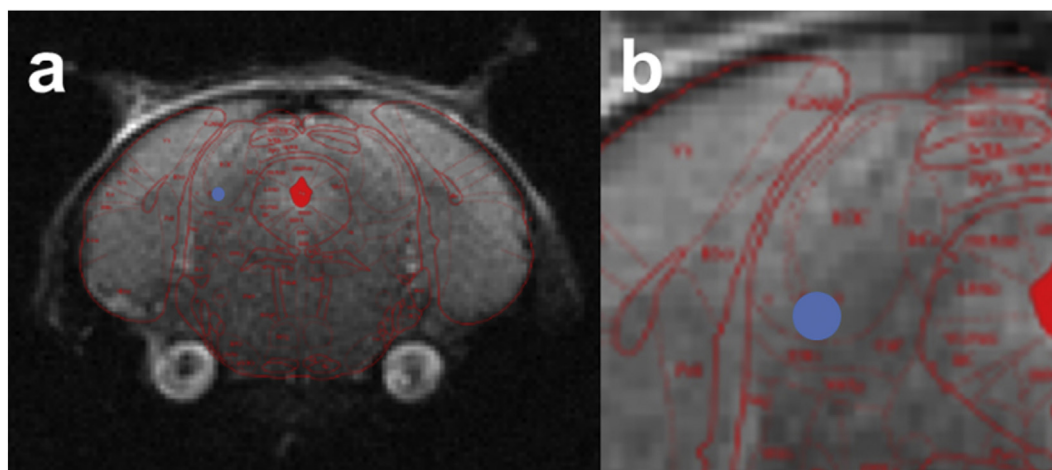

Figure 2. Insertion location of electrode in right hempishere. a) Whole brain coverage of location for probe insertion. Simulated probe location (AP = -4.70 mm Bregma, ML = 1.50mm, and DV = -2.50 mm Bregma).

Ocean Optics). The spectrometer was triggered to acquire 0.9 μs after laser firing with 1 ms acquisition. The spectrometers relayed acquired signals to a computer which produced a graphical presentation of spectral intensity against the corresponding wavelength.

2.5. Data acquisition

Slides were placed in the left/right hemisphere orientation in a sample holder at the LIBS focal point to facilitate rapid positioning. Three consecutive laser pulses were fired per hemisphere and emission spectra recorded. The slide was moved; positions were pre-marked and the LIBS laser/spectrometer were computer controlled to expedite data acquisition. Slides were measured as distance anterior-posterior and registered to the Paxinos & Franklin mouse brain atlas coordinates (Figure 2; Paxinos and Franklin, 2008). The elemental LIBS assessment was performed on tissue sections.

2.6. Data analysis and statistical analysis

To calibrate the wavelength measurement, the spectrometer was calibrated using the argon gas spectrum. The argon spectrum was matched with argon spectral lines available in the Atomic Spectra Database of the National Institute of Standards and Technology (NIST). Raw data from the spectrometer was analyzed using MATLAB (Mathworks, 2017a) with Si spectra of most interest. A baseline correction was performed to subtract background from data by using a median filter. Silicon spectrum lines were also located in the NIST database at various locations with calibrated spectra matched with the database for elemental analysis. Previous reports of Si (I) lines were used for reference: 243.5, 250.69, 251.61, 252.41, 252.85, 263.1, 288.16 (Sola et al., 2017), as well as the Si lines from the NIST database. For each hemisphere on each slide (sectioned at 0.5 mm), the spectra from the three laser pulses were averaged to obtain an average spectrum per hemisphere/slide. The intensity of the entire spectrum was then normalized by that of the 656.2 nm hydrogen line to account for differences in the amount of sample prepared. Each individual slice spectrum used to construct the average spectrum was considered a single sample in a two-sample t-test, and statistical analysis was performed by comparing the intensities of each peak found in the averaged simulated probe silicon group versus the corresponding peak intensity in the control group (saline). An alpha of 0.05 was used for the statistical analysis.

3. Results

Imaging was done to confirm injection location (Figure 2) in order to assist in tissue sectioning. Neuroimaging confirmed section slice of silicon injection (left or right hemisphere) for manual preparation on a tissue block. The full spectra was processed (Figure 3) in order to isolate the specific Si lines (Figure 4). The full spectra and differences can be visualized by Figure 5. Histologically we confirmed the location of our injection (Figure 4a). Subsequently we determined modest silicon expression from the simulated degraded neural probe. Important Si peaks present in the experimental silicon group, but not present in the control saline group, were found 3hr post-injection: Si (I) at 251.6 nm (p = $2.5*10^{-4}$; normalized silicon amplitude = 0.02446; normalized saline amplitude = 0.003386) and Si (I) at 288.2 nm (p = $4.3*10^{-4}$; normalized silicon amplitude = 0.01721; normalized saline amplitude = ~ 0) (Figures 4b and 4c). Neither of these peaks nor any other important Si peaks were found in the 24hr and 1wk condition - only the 3hr injected model found silicon, whereas the 24hr and week had silicon cleared from the tissue (Figure 4b). As silicon cleared within 3 h, we note that perfusion likely reduced levels. We also note that, despite clearance after 3 h, considerable variation in spectra was found (Figure 5a), possibly due to inflammation seen at the 24hr period through histological examination (Figure 5b). Inflammation was found at 24hr as indicated by a macrophage staining of CD68. This could be a sign of early glymphatic
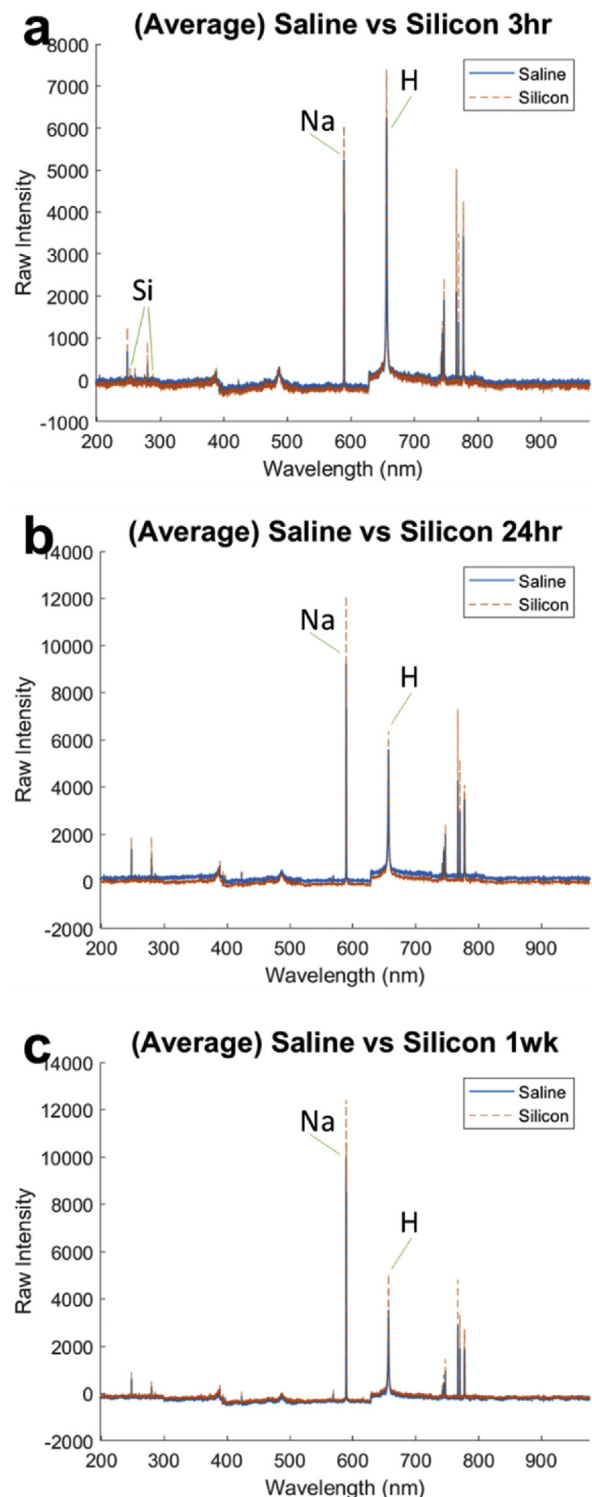

Figure 3. Full average spectra assessed for silicon and saline control. All spectra have been filtered with a median filter to roughly baseline intensity of 0. Data for silicon is in red-orange and data for saline control is in blue. a) LIBS spectra from 3hr silicon and 3hr saline. b) LIBS spectra from 24hr silicon and 24hr saline. c) LIBS spectra from 1-week silicon and 1-week saline.

system involvement. An immune response was not found at 3hr and 1-wk post injection. A heatmap of the LIBS spectra indicated a drastic difference at the 24hr timepoint compared to the 3hr and 1-wk (Figure 5a). We note that LIBS is a very sensitive technique and, even with perfusion, was able to detect miniscule amounts of silicon that remained uncleared after the simulated degraded probe was inserted.
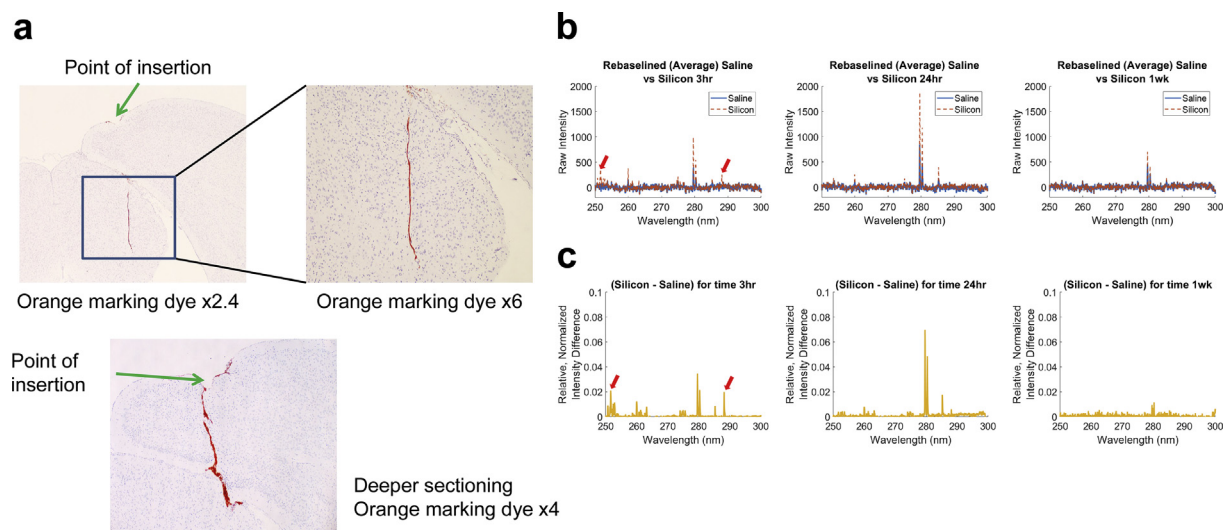
Figure 4. Simulated silicon probe confirmation. a) Orange dye and LFB staining at different magnifications and insert showing detail of injection site. b) LIBS spectra from 3hr, 24hr, and 1-week post-injection in the 250–300 nm region after normalization to the H peak at 656.2 nm. Control saline in blue and silicon groups are in red-orange. For 24hr and 1-week post-injection, no silicon was found; however, silicon peaks were found at 3hr post-injection. c) Difference spectra of silicon and saline data. Note that statistically significant silicon peaks are present for the 3hr post-injection group (indicated by the red arrows in the first graphs in b and c), but were not found to be significant in the 24 h or 1 week post-injection groups. Important peaks found were: Si (I) at 251.6 nm with $p = 2.5*10^{-4}$ and Si (I) at 288.2 nm with $p = 4.3*10^{-4}$.
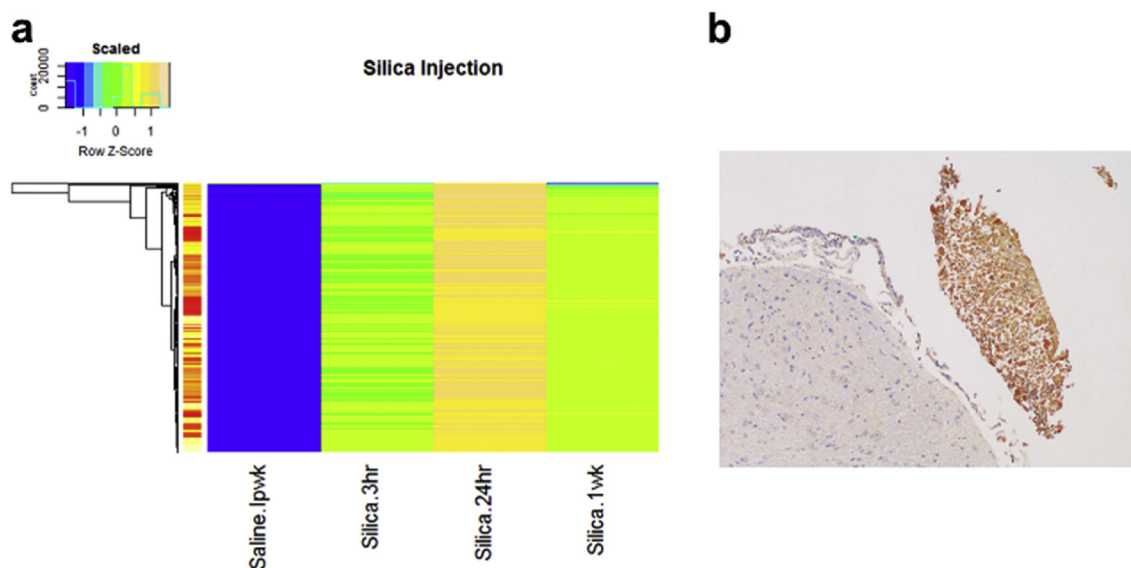

Figure 5. Heatmap of LIBS spectrum results from simulated silicon probe insertion and isolated immune response. a) Heatmap differentiating control (saline group), and silicon groups (3hrs, 24hrs, and 1 wk). The scaled difference is -1 to 1 with silicon 24hr being most different from the control. The immune response at 24hr likely contributed to the greatest difference in the spectra. b) Isolated immune response was found by IHC macrophage staining of CD68 (AB31630). Note the response was isolated and near the inferior colliculus injection site, but located exterior to the needle mark.

4. Discussion

The objective for the present study was to detect and evaluate silicon dispersion from a concentrated source in the mouse brain using laser induced breakdown spectroscopy. Silicon-based neural probes are increasingly used as electrodes for receiving electrical signals from neural tissue. There are three results of considerable interest: First, element lines for Si (I) were found at the injection site at approximately 288 nm at 3hr post-implantation. Second, at 24hr and 1-week post-implantation, no silicon lines were found, indicating clearance, and we suspect this could be a glymphatic clearance. Interestingly, at all timepoints, differences in spectra were found between the silicon and control group. Third, an

isolated immune response was found by CD68 macrophage response at 24hr post injection. Laser induced breakdown spectroscopy can be used to assess silicon uptake by neural tissue and future studies should investigate different tissue states.

Neural probes constructed of silicon are used in electrophysiology (Buzsáki et al., 2015; Gunasekera et al., 2015; Jun et al., 2017; Rivnay et al., 2017) and have been known to potentially induce a chronic neuroinflammatory response (Edell et al., 1992; Turner et al., 1999; Szarowski et al., 2003; Biran et al., 2005, 2007; Skousen et al., 2011). There are several main advantages to using silicon for neural probes: low impedance, good surface adhesion, anticorrosive properties, minimal general inflammatory response in other tissues, and sustained

performance over insertion time (Gunasekera et al., 2015; Jun et al., 2017; Rivnay et al., 2017). However, few protocols have assessed whether silicon diffuses into the brain and elicits an immune response within neural tissue. Here, we have shown that silicon induces an immune response shortly after exposure; we have also demonstrated a protocol using LIBS to assess silicon infusion and dispersal into the brain. Such knowledge is important to consider as preliminary evidence in the development of future chronic electrode implants in humans.

The present manuscript demonstrated silicon can be detected in the brain post injection of a simulated probe using LIBS. Second, we demonstrated that the clearance of silicon, could be through the glymphatic system (e.g. paravascular) or a perivascular pathway (Iliff et al., 2012; Bacyinski et al., 2017). Nevertheless, our present experiment was with a simulated probe bolus, therefore solid-state structural probes could leach silicon in a more time-dependent manner, thus causing continual release. We describe a very effective way to measure probe dissipation and degradation of silicon microelectrodes by measuring the levels of silicon present within neural tissue. The methods described in the present study could be used clinically or in research applications as a post-implantation assay to determine immune response, inflammation, or silicon probe degradation and silicon infusion into the brain. The main advantages of our protocol include robust elemental analysis of biologically relevant states (Ahmed et al., 2017; Ahmed et al., 2018a; Ahmed et al., 2018b; Manno et al., 2018), in addition to easy and consistent sample preparation. For example, in our recent study (Tsui et al., 2020), we measured different single red blood cell (RBC) morphology as induced by titanium dioxide (TiO2) nanoparticle administration. Of interest would be a single cell approach for neural probes to measure silicon probe-tip to neural tissue interfaces. Likewise, single cell approaches using LIBS would be very useful during disease states. The present design can be adapted to measure different neural states; in this study, our overarching aim was to determine silicon dispersion from a putative degraded probe insertion, but similar methods could be used to explore drug perfusion or a variety of other paradigms. We wanted to understand how silicon disperses in the brain from a putative probe injection site, and we have demonstrated the use of LIBS to measure silicon diffusion into the brain after insertion and eventual silicon clearance from neural tissue over a period of several days. The present design could be applied post-implantation to determine whether devices have degraded and potentially had an effect on the electrophysiology or mechanics of the device.

4.1. Study limitations and future directions

The present study used a single bolus of silicon in a neural probe to measure the silicon content dispersal in the brain. Future studies should determine if silicon can continually disperse in the brain during chronic implantation, as silicon is already known to cause inflammation (Biran et al., 2005; Skousen et al., 2011). Future studies should determine whether it is actually the silicon itself causing the immune response or whether the process of foreign material insertion (i.e. the needle or probe) into the brain may lead to the inflammatory response.

5. Conclusion

The present study demonstrated differences in neural characteristics during implantation of a simulated probe. Future studies should determine single neuronal quantitative analyses during different states (as in Tsui et al., 2020), such as disease or during chronic implantation when the probe could be degraded. The use of laser-induced breakdown spectroscopy can be applied to quantify the neural response and the degradation of different neural probes. These include factors like a resulting immune response or differences in the brain parenchyma such as during disease. Future studies will provide valuable preliminary evidence for and potential methods to explore human chronic electrode implants.

Declarations

Competing interest statement

The authors declare no conflict of interest.

Additional information

No additional information is available for this paper.

References

Ahmed, I., Ahmed, R., Yang, J., Law, A.W.L., Zhang, Y., Lau, C., 2017. Elemental analysis of the thyroid by laser induced breakdown spectroscopy. Biomed. Optic Express 8 (11), 4865–4871.

Ahmed, I., Manno, F.A.M., Manno S, H.C., Liu, Y., Zhang, Y., Lau, C., 2018a. Detection of lithium in breast milk and in situ elemental analysis of the mammary gland. Biomed. Optic Express 9 (9), 4184–4195.

Ahmed, I., Yang, J., Law, A.W.L., Manno, F.A.M., Ahmed, R., Zhang, Y., Lau, C., 2018b. Rapid and in situ optical detection of trace lithium in tissues. Biomed. Optic Express 9 (9), 4459–4471.

Bacyinski, A., Xu, M., Wang, W., Hu, J., 2017. The paravascular pathway for brain waste clearance: current understanding, significance and controversy. Front. Neuroanat. 11, 101.

BeMent, S.L., Wise, K.D., Anderson, D.J., Najafi, K., Drake, K.L., 1986. Solid-state electrodes for multichannel multiplexed intracortical neuronal recording. IEEE Trans. Biomed. Eng. 33, 230–241.

Biran, R., Martin, D.C., Tresco, P.A., 2007. The brain tissue response to implanted silicon microelectrode arrays is increased when the device is tethered to the skull. J. Biomed. Mater. Res. 82, 169–178.

Biran, R., Martin, D.C., Tresco, P.A., 2005. Neuronal cell loss accompanies the brain tissue response to chronically implanted silicon microelectrode arrays. Exp. Neurol. 195, 115–126.

Campbell, P.K., Jones, K.E., Huber, R.J., Horch, K.W., Normann, R.A., 1991. A silicon-based, three-dimensional neural interface: manufacturing processes for an intracortical electrode array. IEEE Trans. Biomed. Eng. 38, 758–768.

Collinger, J.L., Wodlinger, B., Downey, J.E., Wang, W., Tyler-Kabara, E.C., Weber, D.J., McMorland, A.J., Velliste, M., Boninger, M.L., Schwartz, A.B., 2013. High-performance neuroprosthetic control by an individual with tetraplegia. Lancet 381 (9866), 557–564.

Dong, C.M., Leong, A.T.L., Manno, F.A.M., Lau, C., Ho, L.C., Chan, R.W., Feng, Y., Gao, P.P., Wu, E.X., 2018. Functional MRI investigation of audiovisual interactions in auditory midbrain. Conf. Proc. IEEE Eng. Med. Biol. Soc. 5527–5530.

Edell, D.J., Toi, V.V., McNeil, V.M., Clark, L.D., 1992. Factors influencing the biocompatibility of insertable silicon microshafts in cerebral cortex. IEEE Trans. Biomed. Eng. 39, 635–643.

Gunasekera, B., Saxena, T., Bellamkonda, R., Karumbaiah, L., 2015. Intracortical recording interfaces: current challenges to chronic recording function. ACS Chem. Neurosci. 6 (1), 68–83.

Hochberg, L.R., Bacher, D., Jarosiewicz, B., Masse, N.Y., Simeral, J.D., Vogel, J., Haddadin, S., Liu, J., Cash, S.S., van der Smagt, P., Donoghue, J.P., 2012. Reach and grasp by people with tetraplegia using a neurally controlled robotic arm. Nature 485 (7398), 372–375.

Hochberg, L.R., Serruya, M.D., Friehs, G.M., Mukand, J.A., Saleh, M., Caplan, A.H., Branner, A., Chen, D., Penn, R.D., Donoghue, J.P., 2006. Neuronal ensemble control of prosthetic devices by a human with tetraplegia. Nature 442 (7099), 164–171.

Hwang, S.W., et al., 2012. A physically transient form of silicon electronics. Science 337, 1640–1644.

Iliff, J.J., Wang, M., Liao, Y., Plogg, B.A., Peng, W., Gundersen, G.A., Benveniste, H., Vates, G.E., Deane, R., Goldman, S.A., Nagelhus, E.A., Nedergaard, M., 2012. A paravascular pathway facilitates CSF flow through the brain parenchyma and the clearance of interstitial solutes, including amyloid β. Sci. Transl. Med. 4 (147), 147ra111.

Jiang, C., Luo, B., Manohar, S., Chen, G.D., Salvi, R., 2017. Plastic changes along auditory pathway during salicylate-induced ototoxicity: hyperactivity and CF shifts. Hear. Res. 347, 28–40.

Jorfi, M., Skousen, J.L., Weder, C., Capadona, J.R., 2015. Progress towards biocompatible intracortical microelectrodes for neural interfacing applications. J. Neural. Eng. 12, 011001.

Jun, J.J., et al., 2017. Fully integrated silicon probes for high-density recording of neural activity. Nature 551 (7679), 232–236.

Kang, S.K., et al., 2016. Bioresorbable silicon electronic sensors for the brain. Nature 530, 71–76.

Kim, S.P., Simerals, J.D., Hochbergs, L.R., Donoghue, J.P., Black, M.J., 2008. Neural control of computer cursor velocity by decoding motor cortical spiking activity in humans with tetraplegia. J. Neural. Eng. 5 (4), 455–476.

Kim, T., Specht, Z.G., Vary, P.S., Lin, C.T., 2004. Spectral fingerprints of bacterial strains by Laser-induced breakdown spectroscopy. J. Phys. Chem. B 108 (17), 5477–5482.

Kumar, A., Yueh, F.Y., Singh, J.P., Burguess, S., 2004. Characterization of malignant tissue cells by laser-induced breakdown spectroscopy. Appl. Optic. 43 (28), 5399–5403.

Lau, C., Manno, F.A.M., Dong, C.M., Chan, K.C., Wu, E.D., 2018. Auditory-visual convergence at the superior colliculus in rat using functional MRI. Conf. Proc. IEEE Eng. Med. Biol. Soc. 5531–5536.

Lorach, H., Goetz, G., Smith, R., Lei, X., Mandel, Y., Kamins, T., Mathieson, K., Huie, P., Harris, J., Sher, A., Palanker, D., 2015. Photovoltaic restoration of sight with high visual acuity. Nat. Methods 21, 476–482.

Mandel, Y., Goetz, G., Lavinsky, D., Huie, P., Mathieson, K., Wang, L., Kamins, T., Galambos, L., Manivanh, R., Harris, J., Palanker, D., 2013. Cortical responses elicited by photovoltaic subretinal prostheses exhibit similarities to visually evoked potentials. Nat. Commun. 4, 1980.

Manno, F.A.M., Isla, A.G., Manno, S.H.C., Ahmed, I., Cheng, S.H., Barrios, F.A., Lau, C., 2019. Neuroimaging the Alzheimer's disease 3xTg mouse model reveals white matter alterations alongside decreased functional connectivity. Front. Aging Neurosci. 11, 39.

Manno, F.A.M., Lau, C., 2018. The pineal gland of the shrew (Blarina brevicauda and Blarina carolinensis): a light and electron microscopic study of pinealocytes. Cell Tissue Res. 374 (3), 595–605.

Manno, S.H.C., Manno, F.A.M., Ahmed, I., Ahmed, R., Shu, L., Li, L., Xu, S., Xie, F., Li, V.W., Ho, J., Cheng, S.H., Lau, C., 2018. Spectroscopic examination of enamel staining by coffee indicates dentin erosion by sequestration of elements. Talanta 89, 550–559.

Mathieson, K., Loudin, J., Goetz, G., Huie, P., Wang, L., Kamins, T.I., Galambos, L., Smith, R., Harris, J.S., Sher, A., Palanker, D., 2012. Photovoltaic retinal prosthesis with high pixel density. Nat. Photon. 6, 391–397.

Mohaidat, Q.I., Sheikh, K., Palchaudhuri, S., Rehse, S.J., 2012. Pathogen identification with laser-induced breakdown spectroscopy: the effect of bacterial and biofluid specimen contamination. Appl. Optic. 51 (7), B99–B107.

Paxinos, G., Franklin, K., 2008. The Mouse Brain in Stereotaxic Coordinates. Compact Academic Press.

Rehse, S.J., Salimnia, H., Miziolek, A.W., 2012. Laser-induced breakdown spectroscopy (LIBS): an overview of recent progress and future potential for biomecial applications. J. Med. Eng. Technol. 36, 77–89.

Rivnay, J., Wang, H., Fenno, L., Deisseroth, K., Malliaras, G.G., 2017. Next-generation probes, particles, and proteins for neural interfacing. Sci. Adv. 3 (6), e1601649.

Skousen, J., Merriam, S.M.E., Srivannavit, O., Perlin, G., Wise, K.D., Tresco, P.A., 2011. Reducing surface area while maintaining implant penetrating profile lowers the brain foreign body response to chronically implanted planar silicon microelectrode arrays. Prog. Brain Res. 194, 167–180.

Sola, D., Paulés, D., Grima, L., Anzano, J., 2017. Laser-induced breakdown spectroscopy (LIBS) for monitoring the formation of hydroxyapatite porous layers. Materials 10 (12), 1395.

Szarowski, D.H., Andersen, M.D., Retterer, S., Spence, A.J., Isaacson, M., Craighead, H.G., Turner, J.N., Shain, W., 2003. Brain responses to micro-machined silicon devices. Brain Res. 983 (1-2), 23–35.

Teran-Hinojosa, E., Sobral, H., Sanchez-Perez, C., Perez-Garcia, A., Aleman-Garcia, N., Hernandez-Ruiz, J., 2017. Differentiation of fibrotic liver tissue using laser-induced breakdown spectroscopy. Biomed. Optic Express 8 (8), 3816–3827.

Tsui, S.M., Ahmed, R., Amjad, N., Ahmed, I., Yang, J., Manno, F.A.M., Barman, I., Shih, W.C., Lau, C., 2020. Single red blood cell analysis reveals elevated hemoglobin in poikilocytes. J. Biomed. Optic. 25 (1), 015004.

Turner, J.N., Shain, W., Szarowski, D.H., Andersen, M., Martins, S., Isaacson, M., Craighead, H., 1999. Cerebral astrocyte response to micromachined silicon implants. Exp. Neurol. 156 (1), 33–49.

Wong, E., Radziwon, K., Chen, G.D., Liu, X., Manno, F.A.M., Manno, S.H.C., Auerbach, B., Wu, E.X., Salvi, R., Lau, C., 2020. Functional magnetic resonance imaging of enhanced central auditory gain and electrophysiological correlates in a behavioral model of hyperacusis. Hear. Res. 389, 107908.

Wise, K.D., Angell, J.B., Starr, A., 1970. An integrated-circuit approach to extracellular microelectrodes. IEEE Trans. Biomed. Eng. 17, 238–247.

Wise, K.D., Angell, J.B., 1975. A low-capacitance multielectrode probe for use in extracellular neurophysiology. IEEE Trans. Biomed. Eng. 22, 212–219.

Yu, K.J., et al., 2016. Bioresorbable silicon electronics for transient spatiotemporal mapping of electrical activity from the cerebral cortex. Nat. Mater. 15, 782–791.

Yueh, F.Y., Zheng, H., Singh, J.P., Burguess, S., 2009. Preliminary evaluation of laser-induced breakdown spectroscopy for tissue classification. Spectrochim. Acta B 64, 1059–1067.

Buzsáki, G., 2015. Hippocampal sharp wave-ripple: A cognitive biomarker for episodic memory and planning. Hippocampus 25 (10), 1073–1188. John Wiley & Sons, Ltd.